Confirming the uniformity of the Hubble flow with Pantheon+ Supernovae

Xiaoyun Shao^{1*} and Carlos A. P. Bengaly^{1†}
¹Observatório Nacional, 20921-400, Rio de Janeiro, RJ, Brazil

According to the perturbed Friedmann model, the difference between Hubble constant measurements in two rest frames, at leading order in velocity, is determined solely by the relative motion of the observers and remains unaffected by the peculiar velocities of the sources. This implies that, when averaging over a sufficiently large and distant set of sources where local nonlinear inhomogeneities are diminished, such a difference should vanish, so that the Hubble flow is statistically uniform, as predicted by the Cosmological Principle - a core assumption of the standard cosmological paradigm. In previous works, distance measurement compilations, e.g. the CosmicFlows-3 catalogue, were used for this purpose, as it comprises a large number ($\sim 10^4$) of sources of different types. Due to the increasing amount of precise luminosity distance measurements of Type Ia Superiovae (SNe) in the last few years, in this work we investigate whether we can confirm the uniformity of the Hubble flow with low-z SN distances only. By means of the Pantheon+ and SH0ES compilation, we find that the results align well with previous works based on the CF3 catalogue, and are in good agreement with the expected Hubble variance in the standard model across cosmic scales of 20-150 Mpc. Notably, the Hubble constant difference $\Delta H_0 \approx 0$ is observed at around 85 Mpc. Despite the smaller sample size ($\sim 10^2$ versus $\sim 10^4$) relative to CF3 at those scales, our analysis show that the Pantheon+ and SH0ES dataset supports the standard model paradigm, which indicates that the Hubble flow becomes statistically uniform at around 70-100 Mpc, which is compatible with independent determinations of the homogeneity scale based on galaxy number

I. INTRODUCTION

The Λ Cold Dark Matter (Λ CDM) model constitutes the prevailing framework in modern cosmology, describing a spatially flat Universe dominated by cold dark matter and dark energy in the form of a cosmological constant. It successfully accounts for a broad range of observations, including the temperature anisotropies of the Cosmic Microwave Background (CMB), large-scale matter clustering probed through weak gravitational lensing, and the luminosity distance-redshift relation of Type Ia supernovae [1–6]. Nevertheless, the Λ CDM framework continues to face unresolved theoretical questions and emerging observational tensions.

The Λ CDM model, while remarkably successful, is not without its theoretical and observational shortcomings. From a theoretical standpoint, challenges such as the coincidence and fine-tuning problems raise concerns about the model's naturalness and underlying assumptions [7]. On the observational front, a persistent tension at the $\sim 5\sigma$ level between early-Universe determinations of the Hubble constant (H_0) and those derived from late-time observations continues to attract significant attention [8, and references therein]. Additionally, recent analyses based on the first two data releases from the Dark Energy Spectroscopic Instrument (DESI) suggest potential deviations from a constant dark energy equation of state, offering possible support for dynamical dark energy models [9, 10]. Nonetheless, these interpretations remain con-

*Electronic address: xiaoyun
48@on.br †Electronic address: carlosbengaly@on.br tentious and continue to be rigorously examined within the scientific community [11–13].

In view of these ongoing challenges, it becomes imperative to verify the validity of the foundational assumptions underlying the ΛCDM model. A central tenet of this framework is the Cosmological Principle (CP), which posits that the Universe is statistically homogeneous and isotropic on sufficiently large scales [14–17]. This principle serves as the basis for the Friedmann-Lemaître-Robertson-Walker (FLRW) metric [18, 19], which underpins the standard cosmological model. However, it is important to emphasize that only statistical isotropy can be directly tested through observations. The assumption of spatial homogeneity remains indirectly inferred, as our observational access is confined to the two-dimensional intersection of our past light cone with the spatial hypersurfaces on which cosmological sources reside. Consequently, tests of homogeneity rely on the internal consistency of observables and cannot be validated through direct measurements.

Several studies suggest that the Universe becomes statistically homogeneous on scales larger than approximately 100 Mpc. However, these estimates can only provide a consistency test of the standard model, as previously discussed, in addition to being limited by the cosmic variance of the corresponding redshift surveys used in those analyses [20–31]. On scales smaller than or comparable to the statistical homogeneity scale, the Hubble flow exhibits a complex pattern of spatial variance. Within the standard FLRW paradigm, such variations are typically interpreted as arising from peculiar velocity fields, i.e., the proper motion of galaxies relative to the uniform Hubble expansion. Those bulk motions are expected to become smaller at larger scales, as the matter density

perturbations decrease. The rest frame defined by the Cosmic Microwave Background serves as the standard frame for comoving observers, anchoring the first-order approximation of the Hubble flow.

Considerable observational effort has been dedicated to understanding peculiar motions in the local Universe. Several studies of peculiar velocities [32–35] have reported persistent bulk flows extending to unexpectedly large scales, potentially challenging the predictions of the perturbed FLRW framework underpinning the standard Λ CDM cosmology. In particular, [36] found that the bulk flow amplitude at a depth of 173 Mpc/h is 428 \pm 108 km/s, significantly exceeding the \sim 192 km/s predicted by Λ CDM mocks. This measurement is in excellent agreement with the independent results of [37], who employed the same methodology and utilized the most recent CosmicFlows-4 (CF4) distance catalogue.

In light of these results, we perform an indirect test of the Cosmological Principle by examining the expansion rate H_0 , computed as a spherically averaged quantity within concentric shells at increasing radial distances. This analysis is influenced by the observer's motion with respect to the cosmic microwave background (CMB) frame, introducing a velocity-dependent effect. According to the CP, the difference in H_0 values averaged over spheres in two distinct rest frames should be independent of both the peculiar velocities of the sources and the observer, as well as of the source distances – assuming the latter are sufficiently large to suppress the impact of local bulk flows arising from nonlinear structure. Due to the significant systematic uncertainties affecting individual H_0 measurements, besides observational limitations e.g. the Malmqist bias, we instead consider the difference in Hubble constants evaluated in two rest frames, which is expected to be negligible at large enough scales if the Cosmological Principle actually holds true [38–42].

Hence, our goal is to verify whether we can confirm the uniformity of the Hubble expansion utilising a single probe of the local universe - namely, the most recent Pantheon+SH0ES Type Ia supernova (SN) compilation [2], which offers more precise distance estimates than the CosmicFlows-3 (CF3) catalog [43]. Although the size of the Pantheon+SH0ES sample is smaller than CF3 by roughly two order of magnitude, our analysis exhibits strong consistency with CF3 measurements within the framework of the standard Λ CDM model over the 20-150 Mpc distance range. In practice, we assess the difference of the Hubble constant H_0 measured in the CMB and Local Group rest frames (hereafter CRF and LRF, respectively) at different cosmic scales as a means to probe the assumption of an uniform Hubble flow from some of these scales onward – and to see if it is consistent with the expectations from a fiducial ΛCDM cosmology. Additionally, we examine the impact of applying CRFand LRF-like velocity boosts in random directions on the reconstructed Hubble flow, in order to perform a complimentary test of its isotropy. A significant deviation in either test could indicate a breakdown of the CP or a departure from the standard cosmological model. However, our results show no evidence of such discrepancies.

The paper is organised as follows. Section II presents the observational dataset and outlines the methodological framework, including the tomographic analysis in spherical shells and the construction of rest-frame differential estimators. Section III details the results of our analysis, including comparisons with Monte Carlo simulations under linear ΛCDM perturbations, tests of statistical isotropy, and the impact of sky coverage. Finally, Section IV provides a comprehensive summary of our findings, discusses their significance in the context of the Cosmological Principle and the standard model, and highlights the prospects of forthcoming surveys.

II. DATA AND METHOD

The Pantheon+SH0ES dataset represents one of the most recent and precise compilation of cosmological distances from SN observations. It encompasses 1701 updated light curves corresponding to 1550 unique SNe, spanning a redshift range from z = 0.001 to 2.26 [44]¹. Among these, 42 SNe Ia are located in galaxies that host Cepheid calibrators, forming the basis for the SH0ES determination of the Hubble constant. This dataset is used in both the Pantheon+ cosmological analysis [2] and the SH0ES H_0 determination [45]. The associated redshifts and peculiar velocity corrections to the SN redshifts are detailed in [46], while a comprehensive modelling of the peculiar velocity field is presented in [47]. This release improves upon the original Pantheon analysis through the incorporation of multiple cross-calibrated photometric systems, an expanded redshift coverage, and refined treatments of systematic uncertainties. These enhancements collectively result in roughly a factor-of-two improvement in the cosmological constraining power.

Figure 1 displays the distribution of Pantheon+SH0ES supernovae across the sky, visualized using the HEALPix scheme [48] at a resolution of Nside = 64. The supernovae are colour-coded by redshift: black points correspond to nearby objects with z < 0.01, blue indicates the intermediate range 0.01 < z < 0.03, and white marks the higher-redshift sample with z > 0.03. At higher redshifts, the non-uniformity in angular coverage becomes increasingly pronounced. We aim to test the consistency between the value of H_0 obtained from the observed Pantheon+SH0ES data in the redshift range z < 0.04, which corresponds to a scale of 150 Mpc, assuming SN redshifts at the LRF and CRF, by the same token as in previous works [38–42].

Data retrieved from the repository https://github.com/ PantheonPlusSHOES/DataRelease.

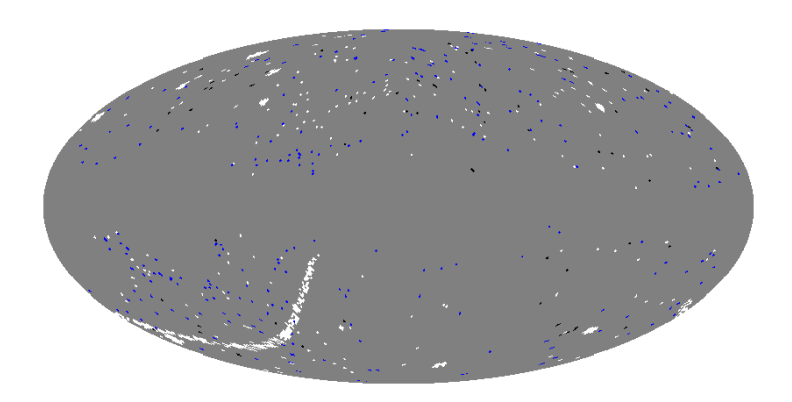


FIG. 1: Mollweide projection showing the sky distribution of Pantheon+SH0ES supernovae: black represents sources with z < 0.01, blue corresponds to 0.01 < z < 0.03, and white denotes z > 0.03.

A. Estimating H_0

For redshifts in the range $z \lesssim 0.05 \, h^{-1}$, the linear approximation of the Hubble law provides a reliable method for estimating the Hubble constant. In this regime, the expansion rate can be expressed as

$$H_0 = \frac{cz}{D(z)} + \mathcal{O}(z^2),\tag{1}$$

where the distance measure D(z) is identified with the luminosity distance $d_L(z)$ once we assume the SN absolute magnitude as $M_B=-19.25\pm0.027$ [45]. This formulation isolates H_0 as the only cosmological parameter of relevance.

Because we restrict our analysis to distances up to roughly 150 Mpc, the higher-order redshift corrections (of order z^2) contribute only at the 2% level-significantly smaller than the typical $\sim 13\%$ uncertainties associated with Pantheon+SH0ES distance measurements. In this low-redshift limit, the distinctions between different cosmological distance definitions (e.g., luminosity, angular diameter, comoving) are negligible. As a result, we omit the $\mathcal{O}(z^2)$ terms in the expressions that follow.

To estimate the Hubble constant, we adopt an approach based on dividing the data into concentric spherical shells, each with a radial thickness of ΔD . Following the method of [42], we choose a broad shell width of $\Delta D=30$ Mpc, which helps reducing the impact of nonlinear motions and allows us to probe larger distances using the Pantheon+SH0ES sample. Within each shell s, containing N_s supernovae, we determine H_0 by minimizing the following chi-squared statistic

$$\chi_s^2 = \sum_{i=1}^{N_s} \left[\frac{D_i - cz_i/H_s}{\sigma_i} \right]^2, \tag{2}$$

This leads to an analytic expression for the best-fit value of the Hubble constant in that shell [38]

$$H_s \equiv H_0|_s = \left[\sum_{i=1}^{N_s} \frac{(cz_i)^2}{\sigma_i^2}\right]^{-1} \left(\sum_{j=1}^{N_s} \frac{cz_j D_j}{\sigma_j^2}\right).$$
 (3)

In these equations, z_i denotes the observed redshift of source i, as measured in the Solar System frame. The quantity $D_i = D(z_i)$ corresponds to its estimated luminosity distance, and σ_i is the uncertainty associated with that distance. All of these quantities are taken directly from the Pantheon+SH0ES dataset.

The average luminosity distance of the N_s sources within shell s, computed as an inverse-variance weighted mean, is given by

$$D_s = \left(\sum_i \frac{D_i}{\sigma_i^2}\right) \left(\sum_j \frac{1}{\sigma_j^2}\right)^{-1},\tag{4}$$

while the associated uncertainty on the estimated Hubble constant ${\cal H}_s$ takes the form

$$\sigma_s^2 = \left[\sum_i \frac{(cz_i)^2}{\sigma_i^2}\right]^3 \left(\sum_j \frac{cz_j D_j}{\sigma_j^2}\right)^{-4}.$$
 (5)

unless otherwise specified, the summations are taken over all sources in the shell, from i = 1 to N_s .

Malmquist bias, a selection effect dependent on distance but not on angular position, can still influence individual estimates of H_s . Rather than analyzing H_s values in isolation within a given rest frame, as done in earlier works such as [38, 39], we adopt the strategy presented in [41], which is based on the difference in H_s values between two rest frames to mitigate such bias. Specifically, we focus on comparing the CMB rest-frame and the Local Group (LG) rest-frame.

The difference in Hubble parameters between frames is defined as

$$\Delta H_s = H_s^{\text{CRF}} - H_s^{\text{LRF}},\tag{6}$$

with an associated uncertainty

$$\sigma_{\Delta H_s}^2 = \left(\sigma_s^{\text{CRF}}\right)^2 + \left(\sigma_s^{\text{LRF}}\right)^2. \tag{7}$$

Since both estimates rely on the same underlying data, the uncertainties in Eq. 7 are likely correlated. Therefore, this expression should be interpreted as an upper limit on the true error in $\Delta H_{\rm c}$.

By substituting redshifts and distances transformed to a specific rest frame (RF) into Eq. 3, we arrive at the corresponding estimator for the Hubble constant

$$H_s^{\rm RF} = \left[\sum_i \frac{(cz_i^{\rm RF})^2}{\sigma_i^2} \right] \left[\sum_j \frac{cz_j^{\rm RF} D^{\rm RF}(z_j^{\rm RF})}{\sigma_j^2} \right]^{-1}. \quad (8)$$

The Solar System's velocity with respect to each reference frame is needed for these transformations. These are

$$v^{\text{CRF}} = 369 \,\text{km/s}, \quad (l^{\text{CRF}}, b^{\text{CRF}}) = (264^{\circ}, 48^{\circ}) \,[49],$$

 $v^{\text{LRF}} = 319 \,\text{km/s}, \quad (l^{\text{LRF}}, b^{\text{LRF}}) = (106^{\circ}, -6^{\circ}) \,[50],$
(9)

where the coordinates (l, b) denote galactic longitude and latitude, respectively.

To leading order in the dimensionless velocity $\beta^{\text{RF}} \equiv \mathbf{v}^{\text{RF}}/c$, the redshift of source i in a given rest frame (RF) is related to the redshift measured in the Solar System frame via

$$z_i^{\text{RF}} = z_i + (1 + z_i) \,\mathbf{n}_i \cdot \boldsymbol{\beta}^{\text{RF}}.\tag{10}$$

In a general spacetime, the Doppler-induced correction to the luminosity distance takes the form [51]

$$D^{RF}(z_i^{RF}, \mathbf{n}_i) = D(z_i, \mathbf{n}_i) \left[1 + \mathbf{n}_i \cdot \boldsymbol{\beta}^{RF} \right], \tag{11}$$

where $\mathbf{n}_i^{\mathrm{RF}}$ is the aberration of direction. The effect of the source's peculiar velocity $\boldsymbol{\beta}_i$ is included in the function $D(z_i, \mathbf{n}_i)$. In a linearly perturbed Friedmann model, the observed luminosity distance in the Solar System frame relates to the background value $\bar{D}(z_i)$ as [52, 53]:

$$D(z_i, \mathbf{n}_i) = \bar{D}(z_i) \left[1 + A_i \, \mathbf{n}_i \cdot \boldsymbol{\beta}^{\text{CRF}} + (1 - A_i) \, \mathbf{n}_i \cdot \boldsymbol{\beta}_i \right]$$

$$A_i \equiv \frac{(1 + z_i)^2}{\bar{D}(z_i) H(z_i)}.$$
(12)

Following the approach of [42], we can obtain the expression for ΔH_s under the assumption of a linear Hubble law for the background luminosity distance

$$\Delta H_s = \frac{H_0}{L_s} \sum_i \frac{c^2 z_i}{\sigma_i^2} \boldsymbol{n}_i \cdot \left(\boldsymbol{\beta}^{\text{CRF}} - \boldsymbol{\beta}^{\text{LRF}} \right), \qquad (13)$$

where $L_s \equiv \sum_i (cz_i)^2/\sigma_i^2$. Notably, contributions from the peculiar velocities β_i cancel out at first order in the difference between reference frames, as they are frame-independent.

Importantly, Eq. 13 implies that if all sources within shell s share the same redshift and uncertainty, the sum reduces to a directional average. For an isotropic distribution of sources over the sky, this average vanishes, resulting in $\Delta H_s = 0$. However, in realistic cases where sources have varying redshifts and uncertainties within

the shell, the summation no longer cancels, and ΔH_s acquires a nonzero value – even for an underlying isotropic distribution. This behaviour is redshift-dependent, and the general trend follows

$$\frac{|\Delta H_s|}{H_0} \quad \begin{cases} \text{grows as } z_s \to 0 \\ \to 0 \text{ as } z_s \text{ grows} \end{cases}$$
 (14)

An important advantage of this analysis is that the redshifts z_i are directly observed quantities, without relying on any underlying ΛCDM assumptions. At low redshift, they inherently capture anisotropies and nonlinear effects, such as local bulk flows, which are expected features of structure formation in a ΛCDM universe [41]. Although our formalism is based on a linear Doppler approximation for rest-frame transformations, it does not eliminate the nonlinear signatures encoded in the observed redshifts.

B. Consistency Tests

To assess the consistency of the Pantheon+SH0ES results with the standard Λ CDM cosmology, we perform two independent sets of 1,000 Monte Carlo (MC) simulations. Each mock catalogue preserves the angular coordinates of the original supernovae, thereby reproducing the non-uniform sky coverage inherent to the Pantheon+SH0ES dataset. The methodology for generating these simulations is outlined as follows

• MC-ACDM: For each supernova in the Pantheon+SH0ES sample, we generate a mock luminosity distance by sampling from a Gaussian distribution:

$$D_i^{\text{MC}} \sim \mathcal{N}(\bar{D}_i, \sigma_i),$$
 (15)

where \bar{D}_i denotes the expected distance predicted by a fiducial ΛCDM model, and σ_i represents the observational uncertainty, as provided in the original data release. To mimic the effect of changing reference frames, both redshifts and distances are transformed according to the prescriptions given in Eqs. 10 and 11.

• MC-Boost: In this set, we apply CMB- and LG-like boosts to the redshift and distance of each supernova. While their amplitudes are fixed to v^{CRF} and v^{LRF} , their directions are randomised using angular coordinates $(l^{\text{MC}}, b^{\text{MC}})$. The boosted redshifts are computed as follows

$$cz_{i}^{\text{MC,CRF}} = cz_{i} + 369 \left[\cos b_{i} \cos b^{\text{MC}} + \sin b_{i} \sin b^{\text{MC}} \cos(l_{i} - l^{\text{MC}}) \right],$$

$$cz_{i}^{\text{MC,LRF}} = cz_{i} + 319 \left[\cos b_{i} \cos b^{\text{MC}} + \sin b_{i} \sin b^{\text{MC}} \cos(l_{i} - l^{\text{MC}}) \right].$$
(16)

The angular coordinates defining the boost directions are drawn from uniform distributions over the full celestial sphere

$$b^{\text{MC}} \sim \arcsin(-\pi/2 + \pi \mathcal{U}[0, 1]), \quad l^{\text{MC}} \sim \mathcal{U}[0, 2\pi].$$
 (17)

III. RESULTS

A. ΔH_s from the Pantheon+SH0ES

$D_{\min} = 20$	D_s	Shells	ΔH_s	$2\sigma_{\Delta H_s}$
(Mpc)	(Mpc)	(Mpc)	(km/s/Mpc)	(km/s/Mpc)
-	31.37	$20 \le D \le 50$	4.04	3.21
	63.59	$50 \le D \le 80$	-2.13	2.23
	94.63	$80 \le D \le 110$	0.18	1.72
	124.37	$110 \leq D \leq 140$	-0.46	1.81
$D_{\min} = 30$	D_s	Shells	ΔH_s	$2\sigma_{\Delta H_s}$
(Mpc)	(Mpc)	(Mpc)	(km/s/Mpc)	(km/s/Mpc)
-	42.72	$30 \le D \le 60$	-0.10	2.80
	73.42	$60 \le D \le 90$	-1.42	2.09
	102.38	$90 \le D \le 120$	0.01	1.70
	133.32	$120 \leq D \leq 150$	-0.59	1.87
$D_{\min} = 40$	D_s	Shells	ΔH_s	$2\sigma_{\Delta H_s}$
(Mpc)	(Mpc)	(Mpc)	(km/s/Mpc)	(km/s/Mpc)
-	56.11	$40 \le D \le 70$	-2.22	2.53
	85.53	$70 \le D \le 100$	-0.06	1.85
	113.25	$100 \leq D \leq 130$	-0.37	1.78

TABLE I: Respectively, we present the tabulated values of the weighted average shell radius D_s and the shell boundaries, along with the ΔH_s values and their associated uncertainties obtained from the Pantheon+SH0ES dataset, evaluated at $D_{\rm min}=20,\,30,\,{\rm and}\,40$ Mpc.

As shown in Fig. 2, the difference in the Hubble constant, $\Delta H_s = H_s^{\rm CRF} - H_s^{\rm LRF}$, is plotted as a function of the weighted average shell distance D_s for the Pantheon+SH0ES in red. We also plot the results obtained from the CosmicFlows-3 (CF3) dataset in blue, for the sake of comparison, taken from Table 1 of [42]. The Pantheon+SH0ES values are computed according to the methodology detailed in Sec. II A, using successive radial shells of width $\Delta D = 30$ Mpc. The corresponding numerical results are presented in Table I.

Each point reflects the estimated ΔH_s for a given shell, with vertical error bars representing 2σ uncertainties. While Pantheon+SH0ES exhibits larger statistical errors due to its smaller sample size, both datasets show consistent trends as expected in our analytical expectation in Eq.14.

A notable discrepancy between the Hubble constant estimates in the CMB and LG rest frames is evident at small scales, particularly for $D_s \lesssim 30\,\mathrm{Mpc}$, where the observed values of ΔH_s are systematically positive. This result is in line with earlier studies, which indicate a more uniform in the Hubble flow in the LRF compared to the CRF [38, 39]. As the shell radius increases, the magnitude of ΔH_s diminishes and gradually approaches

zero, consistent with linear theory predictions and the expected emergence of large-scale statistical isotropy as the impact of local structures becomes smaller.

While the 2σ confidence intervals for $D_s > 30\,\mathrm{Mpc}$ are broad enough to include zero, the point estimates for ΔH_s are statistically indistinguishable from zero only beyond $D_s \gtrsim 85\,\mathrm{Mpc}$. This transition scale is in agreement with independent determinations of the homogeneity scale based on galaxy number counts [20–31].

B. ΔH_s from the MC realisations

Fig. 3 displays the simulated ΔH_s values obtained from the MC realisations. The light blue and light red shaded regions represent the MC- Λ CDM and MC-boost ensembles, respectively. Each shaded band is centered on the median best-fit ΔH_s across all realisations, with its width corresponding to the median $2\sigma_{\Delta H_s}$ uncertainty. Observational results, previously presented in Fig. 2, are shown with 2σ error bars for three different minimum-distance thresholds: $D_{\rm min} > 20$ Mpc (red), > 30 Mpc (blue), and > 40 Mpc (magenta). The results demonstrate that the ΔH_s values inferred from the MC simulations are statistically consistent with those from the observed data at all distance scales, within the 2σ confidence interval.

In the case of the MC-boost test, its concordance with respect to the observed data suggests that the CMB and LG rest frames do not exhibit statistically significant deviations from the ensemble of 1,000 randomly oriented frames, providing no compelling evidence for a violation of statistical isotropy in the local Universe

In the MC- Λ CDM test, the results also show reasonable agreement with the observational data, even on mildly nonlinear scales. This is expected, as the linear Doppler-based analysis employed here operates directly on observed redshifts, which already encapsulate the impact of local bulk motions, as detailed in Sec. II A. However, for $D_{\rm min} < 20$ Mpc, the limitations of the linear approximation become significant, and a fully nonlinear treatment, such as that provided by N-body simulations, would be necessary to accurately model the dynamics in this regime [41].

We additionally generated isotropic MC- Λ CDM and MC-boost realisations, i.e., we uniformly redistributed the source positions across the celestial sphere, instead of retaining their original angular distribution. This approach enables us to assess the impact of non-uniform sky coverage on our results. The corresponding outcomes, presented in Fig. 4, are consistent with those obtained from the Pantheon+SH0ES dataset and the original MC realisations. These findings indicate that the non-uniform angular distribution of sources in the observational data does not introduce significant bias into our analysis.

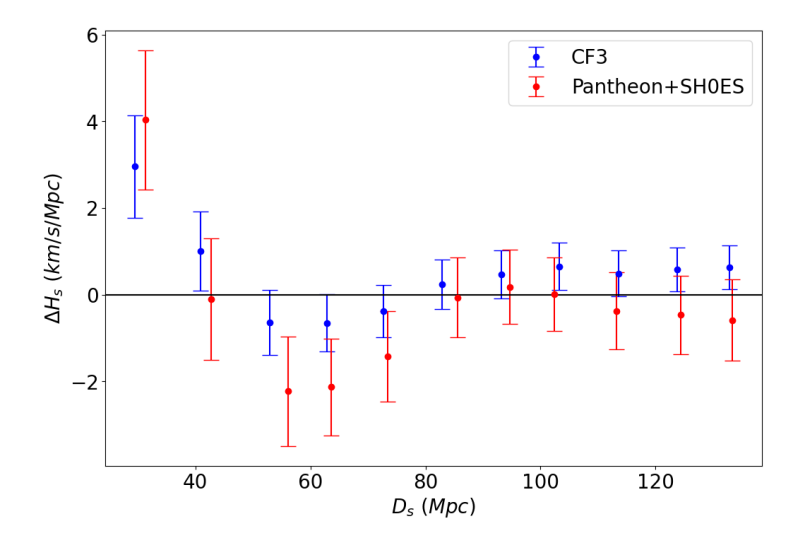


FIG. 2: Difference in the average Hubble constant, ΔH_s , between the CMB and Local Group rest frames for Pantheon+SH0ES and CF3 dataset, shown as a function of shell-averaged distance D_s . The values are computed in successive spherical shells of width $\Delta D = 30$ Mpc, with minimum distances of 20, 30, and 40 Mpc. The error bars represent 2σ uncertainties. Numerical values are listed in Table 1.

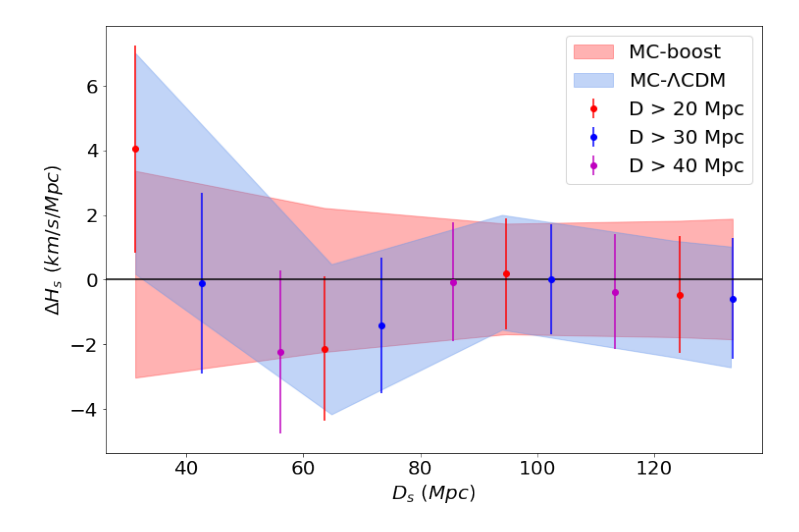


FIG. 3: Comparison of the differential Hubble constant, ΔH_s , between the CMB and LG rest frames based on 1,000 MC realisations. The results from observational data are contrasted with two simulated ensembles: the MC-boost realisations (shaded in light red) and the MC- Λ CDM realisations (shaded in light blue). The shaded bands represent the median ΔH_s trend across all realisations, with widths defined by the corresponding median $2\sigma_{\Delta H_s}$ uncertainties.

IV. CONCLUSIONS

We investigated the uniformity of the local Hubble flow by analysing the most recent and precise compilation of Type Ia Supernova cosmological distances, namely the Pantheon+SH0ES dataset. Despite its smaller sample size compared to compilation of cosmological distance measurements obtained through different methods (not only standardisable candles), as the case of the CosmicFlows-3 catalogue, the Supernova distances reported in this dataset exhibit much smaller uncertainties – so, we expect that they should be able to capture the transition from a locally lumpy universe to

a smoothed-out, statistically homogeneous one, as predicted by the cosmological principle within the standard model paradigm.

Our analysis was carried out by fitting a linear Hubble law in tomographic radial shells within a shell width of $\Delta D_s = 30$ Mpc to reduce statistical noise, following the methodology introduced in [38] and further developed in [39, 41]. Rather than examining absolute H_0 values in individual rest frames, we focused on the differential quantity $\Delta H_s = H_s^{\rm CRF} - H_s^{\rm LRF}$, which mitigates the impact of Malmquist bias and avoids the need to apply further corrections relative to a fiducial background value of H_0 . According to the approach of [42], within

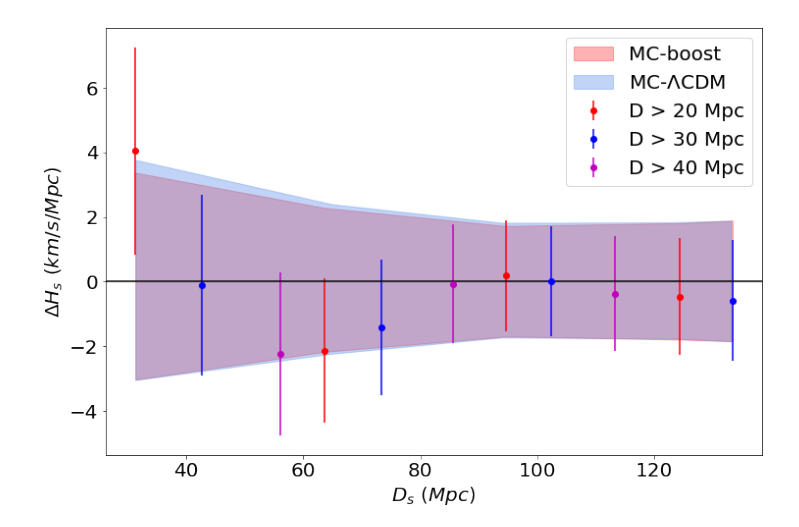


FIG. 4: Same as Fig. 3, but showing results for uniformly distributed Monte Carlo realisations.

the context of a linearly perturbed Friedmann–Lemaître–Robertson–Walker spacetime, it is expected that ΔH_s becomes negligible (even if nonzero, due to the uneven distribution of sources within a given ΔD_s shell) as z_s increases. Hence, any deviation from this result would hint at a possible breakdown of the cosmological principle – and thus the standard cosmological model – by means of a non-uniform Hubble flow at large scales.

As illustrated in Fig. 3, the Monte Carlo simulations constructed under the linear perturbation regime of the Λ CDM model (MC- Λ CDM) yield results that are statistically consistent with the observational data within the 2σ confidence bounds. We further verified that our findings are compatible with Monte Carlo realisations incorporating randomly oriented CMB- and LG-like boosts, which supports the absence of significant deviations from statistical isotropy. Moreover, the consistency with simulations based on uniformly distributed sources indicates that the incompleteness in the sky coverage of the Pantheon+SH0ES dataset does not introduce significant bias into our analysis.

Therefore, we are able confirm the conclusions previously reached in [39] and [42], i.e., that the Hubble flow indeed appears to become uniform at scales of 70-100 Mpc – but using Supernova observations only for the first time. Interestingly, our results agree with the homogeneity scale estimated from redshift surveys, showing that there is an interplay between them – which helps strengthen the observational evidence for the cosmological principle.

In the future, we expect that observational tests of the Hubble flow uniformity should be significantly improved in light of several upcoming surveys that are expected to provide significantly enhance peculiar velocity (PV) measurements [54]

• DESI PV will exploit spare fibres from the main DESI survey to obtain $\sim 133{,}000$ Fundamental Plane (FP) and $\sim 53{,}000$ Tully-Fisher (TF) dis-

tances using optical spectroscopy, becoming the first large-scale survey to measure both FP and TF distances with the same instrument.

- WALLABY, a radio survey using ASKAP, will cover $14{,}000~deg^2$ in the southern sky over 0 < z < 0.1, yielding tens of thousands of HI-based TF distances.
- 4MOST Hemisphere Survey (4HS) will provide spectra for ~ 6 million galaxies over 17,000 deg^2 in the southern hemisphere, including $\sim 400,000$ FP distances for early-type galaxies, forming the largest FP sample to date.
- ZTF and LSST will vastly expand Type Ia supernova (SNe Ia) datasets. ZTF targets low-redshift SNe Ia (z < 0.06, currently $\sim 3,600$ events), while LSST will detect millions of SNe Ia up to z < 0.35, ideal for probing PVs at intermediate redshifts where SNe Ia are the only reliable tracers.

Appendix A: Pantheon+ compilation without SH0ES

For the sake of completeness, we also perform this analysis using the Pantheon+ Type Ia supernova compilation with the SH0ES subsample excluded. As shown in Fig. 5 and Fig. 6, the results remain consistent with those obtained using the Pantheon+ dataset with SH0ES included. No significant deviations are observed that would suggest a violation of the Cosmological Principle or a departure from the standard Λ CDM model.

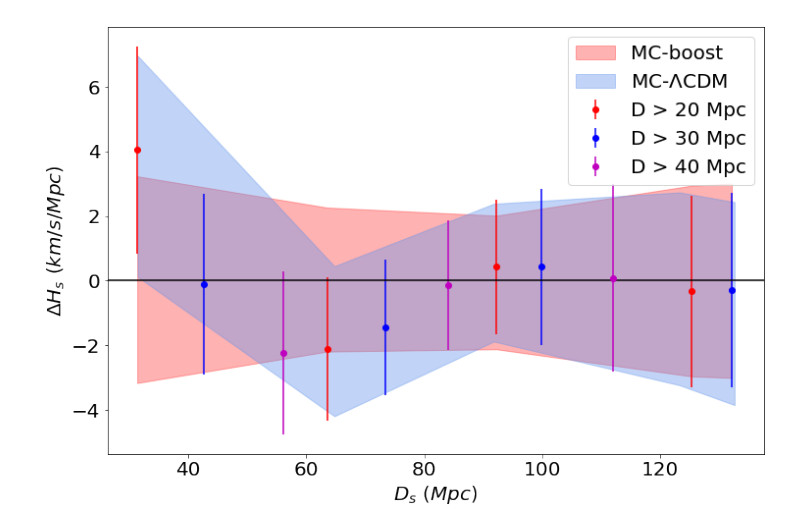


FIG. 5: Same as Fig. 3, but for Pantheon+ compilation exclude SH0ES instead.

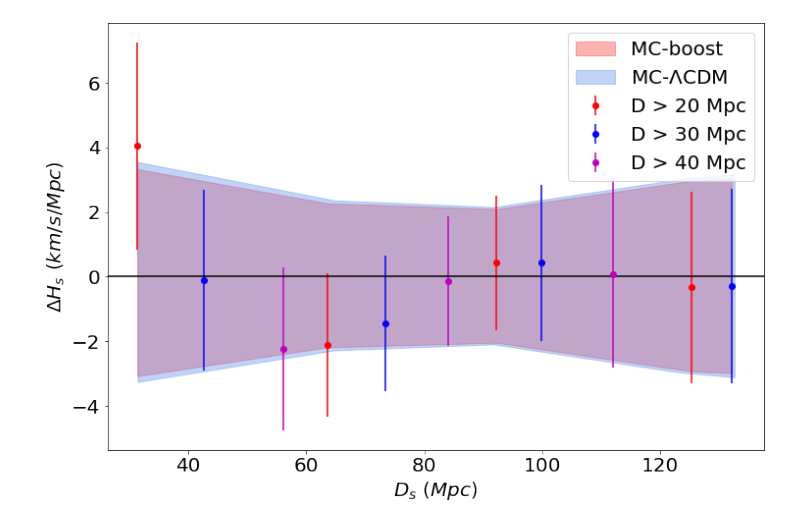


FIG. 6: Same as Fig. 4, but for Pantheon+ compilation exclude SH0ES instead.

Appendix B:
$$\Delta H_s = H_s^{\text{HD}} - H_s^{\text{LRF}}$$

As shown in Fig. 7, we compare the differential Hubble parameter $\Delta H_s = H_s^{\rm CRF} - H_s^{\rm LRF}$ across several datasets: the Pantheon+ Type Ia supernova compilation including SH0ES (green), Pantheon+ excluding SH0ES (cyan), and the CF3 catalog (blue). The results are in good agreement across the different samples, indicating robustness with respect to dataset selection. Additionally, we compute $\Delta H_s = H_s^{\rm HD} - H_s^{\rm LRF}$ (red), where $H_s^{\rm HD}$ is derived using the Hubble diagram redshift $z_{\rm HD}$, which is calibrated to account for both the observer's motion in the CMB frame and the peculiar velocities of the sources. Notably, the ΔH_s values based on $z_{\rm HD}$ lie closer to zero and exhibit reduced scatter, suggesting a more uniform Hubble flow compared to the results obtained using $z_{\rm CMB}$ with the SH0ES-included Pantheon+ dataset.

Appendix C: Stability of ΔH_s Under Variations in Fiducial Cosmology

We have also confirmed the robustness of our results under a fiducial cosmology consistent with the Planck 2018 Λ CDM best-fitted parameters [1] for the MC- Λ CDM simulations. As illustrated in Fig. 8 and Fig. 9, our conclusions remain stable under this cosmology and are not significantly affected by small variations in the underlying cosmological parameters. The results remain in good agreement with those obtained using the Pantheon+ fiducial cosmology, further supporting the consistency of our findings.

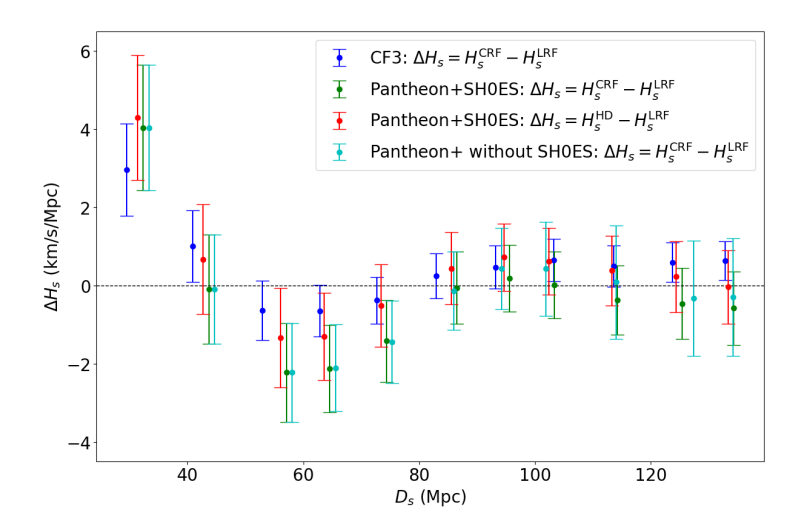


FIG. 7: Difference in the average Hubble constant ΔH_s as a function of shell distance D_s , relative to the local rest frame, using various datasets and redshift definitions. Blue points show CF3 results with $\Delta H_s = H_s^{\rm CRF} - H_s^{\rm LRF}$; green and cyan points show Pantheon+ results using $z_{\rm CRF}$, with and without SH0ES, respectively; red points use the Hubble diagram redshift $z_{\rm HD}$, with $\Delta H_s = H_s^{\rm HD} - H_s^{\rm LRF}$.

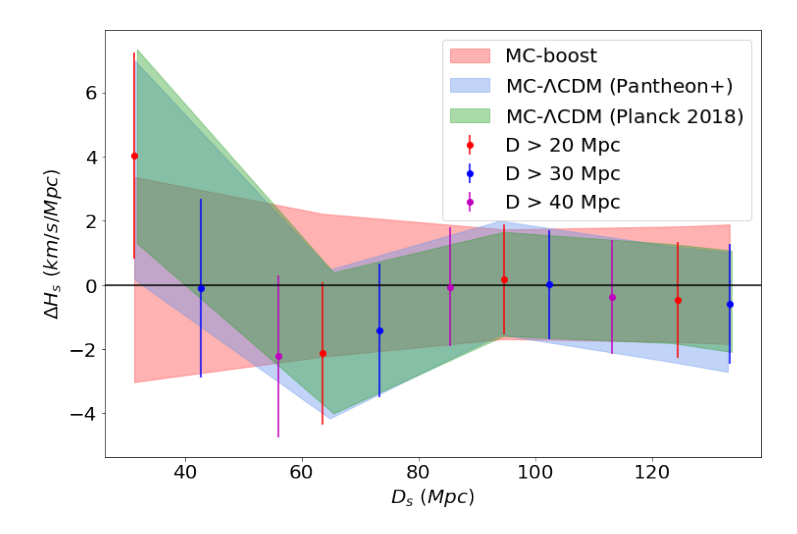


FIG. 8: Same as Fig. 3, but using a fiducial cosmology based on the Planck 2018 parameters [1].

Acknowledgements

XS acknowledges financial support by FAPERJ Doutorado Nota 10 fellowship, besides CAPES at the

early stage of this work. CB acknowledges financial support from the CNPq grant 306630/2025-7. Some of the analysis carried out in this work made use of HEALPix.

^[1] N. Aghanim et al. Planck 2018 results. VI. Cosmological parameters. *Astron. Astrophys.*, 641:A6, 2020. [Erratum: Astron.Astrophys. 652, C4 (2021)].

^[2] Dillon Brout et al. The Pantheon+ Analysis: Cosmological Constraints. *Astrophys. J.*, 938(2):110, 2022.

^[3] Shadab Alam et al. Completed SDSS-IV extended Baryon Oscillation Spectroscopic Survey: Cosmological implications from two decades of spectroscopic surveys at the Apache Point Observatory. *Phys. Rev. D*,

^{103(8):083533, 2021.}

^[4] T. M. C. Abbott et al. Dark Energy Survey Year 3 results: Cosmological constraints from galaxy clustering and weak lensing. *Phys. Rev. D*, 105(2):023520, 2022.

^[5] Mathew S. Madhavacheril et al. The Atacama Cosmology Telescope: DR6 Gravitational Lensing Map and Cosmological Parameters. Astrophys. J., 962(2):113, 2024.

^[6] Xiangchong Li et al. Hyper Suprime-Cam Year 3 results: Cosmology from cosmic shear two-point correlation func-

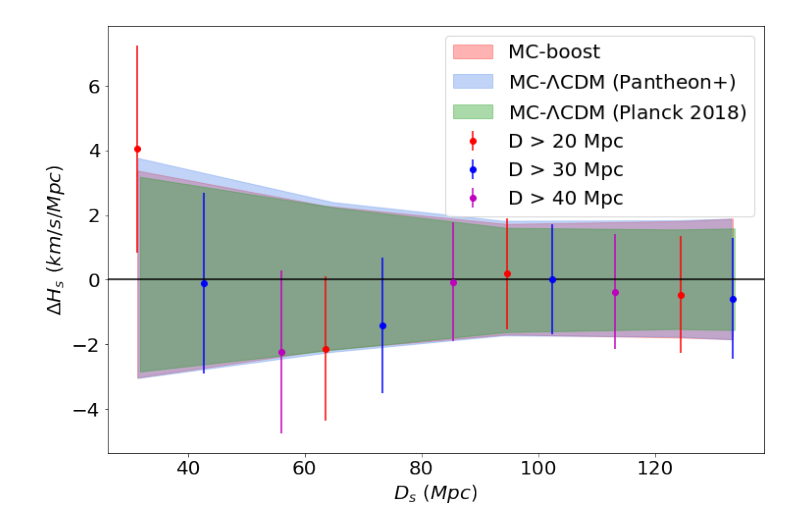


FIG. 9: Same as Fig. 4, but adopting the Planck 2018 cosmological parameters.

- tions. Phys. Rev. D, 108(12):123518, 2023.
- [7] Steven Weinberg. The Cosmological constant problems. In 4th International Symposium on Sources and Detection of Dark Matter in the Universe (DM 2000), pages 18–26, 2 2000.
- [8] Eleonora Di Valentino, Olga Mena, Supriya Pan, Luca Visinelli, Weiqiang Yang, Alessandro Melchiorri, David F. Mota, Adam G. Riess, and Joseph Silk. In the realm of the Hubble tension—a review of solutions. Class. Quant. Grav., 38(15):153001, 2021.
- [9] A. G. Adame et al. DESI 2024 VI: cosmological constraints from the measurements of baryon acoustic oscillations. *JCAP*, 02:021, 2025.
- [10] K. Lodha et al. Extended dark energy analysis using DESI DR2 BAO measurements. Phys. Rev. D, 112(8):083511, 2025.
- [11] Marina Cortês and Andrew R. Liddle. Interpreting DESI's evidence for evolving dark energy. JCAP, 12:007, 2024.
- [12] Purba Mukherjee and Anjan Ananda Sen. Model-independent cosmological inference post DESI DR1 BAO measurements. *Phys. Rev. D*, 110(12):123502, 2024.
- [13] Agripino Sousa-Neto, Carlos Bengaly, Javier E. Gonzalez, and Jailson Alcaniz. Symbolic regression analysis of dynamical dark energy with DESI-DR2 and SN data. *Phys. Dark Univ.*, 50:102108, 2025.
- [14] Chris Clarkson and Roy Maartens. Inhomogeneity and the foundations of concordance cosmology. Class. Quant. Grav., 27:124008, 2010.
- [15] Roy Maartens. Is the Universe homogeneous? Phil. Trans. Roy. Soc. Lond. A, 369:5115–5137, 2011.
- [16] Chris Clarkson. Establishing homogeneity of the universe in the shadow of dark energy. Comptes Rendus Physique, 13:682–718, 2012.
- [17] Pavan Kumar Aluri et al. Is the observable Universe consistent with the cosmological principle? Class. Quant. Grav., 40(9):094001, 2023.
- [18] Stephen W. Hawking and George F. R. Ellis. The Large Scale Structure of Space-Time. Cambridge Monographs on Mathematical Physics. Cambridge University Press, 2 2023.
- [19] Steven Weinberg. Cosmology. 2008.

- [20] David W. Hogg, Daniel J. Eisenstein, Michael R. Blanton, Neta A. Bahcall, J. Brinkmann, James E. Gunn, and Donald P. Schneider. Cosmic homogeneity demonstrated with luminous red galaxies. *Astrophys. J.*, 624:54–58, 2005.
- [21] Morag Scrimgeour et al. The WiggleZ Dark Energy Survey: the transition to large-scale cosmic homogeneity. Mon. Not. Roy. Astron. Soc., 425:116–134, 2012.
- [22] David Alonso, Ana Isabel Salvador, Francisco Javier Sánchez, Maciej Bilicki, Juan García-Bellido, and Eusebio Sánchez. Homogeneity and isotropy in the Two Micron All Sky Survey Photometric Redshift catalogue. Mon. Not. Roy. Astron. Soc., 449(1):670–684, 2015.
- [23] Pierre Laurent et al. A $14 h^{-3}$ Gpc³ study of cosmic homogeneity using BOSS DR12 quasar sample. *JCAP*, 11:060, 2016.
- [24] Pierros Ntelis et al. Exploring cosmic homogeneity with the BOSS DR12 galaxy sample. JCAP, 06:019, 2017.
- [25] R. S. Gonçalves, G. C. Carvalho, C. A. P. Bengaly, J. C. Carvalho, A. Bernui, J. S. Alcaniz, and R. Maartens. Cosmic homogeneity: a spectroscopic and model-independent measurement. *Mon. Not. Roy. Astron. Soc.*, 475(1):L20–L24, 2018.
- [26] R. S. Gonçalves, G. C. Carvalho, C. A. P. Bengaly, J. C. Carvalho, and J. S. Alcaniz. Measuring the scale of cosmic homogeneity with SDSS-IV DR14 quasars. Mon. Not. Roy. Astron. Soc., 481(4):5270–5274, 2018.
- [27] Rodrigo S. Gonçalves, Gabriela C. Carvalho, Uendert Andrade, Carlos A. P. Bengaly, Joel C. Carvalho, and Jailson Alcaniz. Measuring the cosmic homogeneity scale with SDSS-IV DR16 Quasars. JCAP, 03:029, 2021.
- [28] Uendert Andrade, Rodrigo S. Gonçalves, Gabriela C. Carvalho, Carlos A. P. Bengaly, Joel C. Carvalho, and Jailson Alcaniz. The angular scale of homogeneity with SDSS-IV DR16 luminous red galaxies. *JCAP*, 10:088, 2022.
- [29] Xiaoyun Shao, Rodrigo S. Gonçalves, Carlos A. P. Bengaly, Uendert Andrade, Gabriela C. Carvalho, and Jailson Alcaniz. Can the angular scale of cosmic homogeneity be used as a cosmological test? Eur. Phys. J. C, 84(7):655, 2024.
- [30] Xiaoyun Shao, Carlos A. P. Bengaly, Rodrigo S.

- Gonçalves, Gabriela C. Carvalho, and Jailson Alcaniz. Cosmological constraints from angular homogeneity scale measurements. *Eur. Phys. J. C*, 85(3):225, 2025.
- [31] Priya Goyal, Sunil Malik, Jaswant k. Yadav, and T. R. Seshadri. Investigating cosmic homogeneity using multi-fractal analysis of the SDSS-IV eBOSS DR16 quasar catalogue. Mon. Not. Roy. Astron. Soc., 530(3):2866–2876, 2024.
- [32] Richard Watkins, Hume A. Feldman, and Michael J. Hudson. Consistently Large Cosmic Flows on Scales of 100 Mpc/h: a Challenge for the Standard LCDM Cosmology. Mon. Not. Roy. Astron. Soc., 392:743-756, 2009.
- [33] Hume A. Feldman, Richard Watkins, and Michael J. Hudson. Cosmic Flows on 100 Mpc/h Scales: Standardized Minimum Variance Bulk Flow, Shear and Octupole Moments. Mon. Not. Roy. Astron. Soc., 407:2328–2338, 2010.
- [34] A. Kashlinsky, F. Atrio-Barandela, D. Kocevski, and H. Ebeling. A measurement of large-scale peculiar velocities of clusters of galaxies: results and cosmological implications. *Astrophys. J. Lett.*, 686:L49–L52, 2009.
- [35] A. Kashlinsky, F. Atrio-Barandela, H. Ebeling, A. Edge, and D. Kocevski. A new measurement of the bulk flow of X-ray luminous clusters of galaxies. *Astrophys. J. Lett.*, 712:L81–L85, 2010.
- [36] Abbé M. Whitford, Cullan Howlett, and Tamara M. Davis. Evaluating bulk flow estimators for CosmicFlows-4 measurements. Mon. Not. Roy. Astron. Soc., 526(2):3051-3071, 2023.
- [37] Richard Watkins, Trey Allen, Collin James Bradford, Albert Ramon, Alexandra Walker, Hume A. Feldman, Rachel Cionitti, Yara Al-Shorman, Ehsan Kourkchi, and R. Brent Tully. Analysing the large-scale bulk flow using cosmicflows4: increasing tension with the standard cosmological model. Mon. Not. Roy. Astron. Soc., 524(2):1885–1892, 2023.
- [38] David L. Wiltshire, Peter R. Smale, Teppo Mattsson, and Richard Watkins. Hubble flow variance and the cosmic rest frame. *Phys. Rev. D*, 88:083529, 2013.
- [39] James H. McKay and David L. Wiltshire. Defining the frame of minimum non-linear Hubble expansion variation. Mon. Not. Roy. Astron. Soc., 457(3):3285–3305, 2016. [Erratum: Mon.Not.Roy.Astron.Soc. 463, 3113 (2016)].
- [40] Krzysztof Bolejko, M. Ahsan Nazer, and David L. Wiltshire. Differential cosmic expansion and the Hubble flow anisotropy. JCAP, 06:035, 2016.
- [41] David Kraljic and Subir Sarkar. Frames of most uniform Hubble flow. JCAP, 10:016, 2016.

- [42] Carlos A. P. Bengaly, Julien Larena, and Roy Maartens. Is the local Hubble flow consistent with concordance cosmology? *JCAP*, 03:001, 2019.
- [43] R. Brent Tully, Helene M. Courtois, and Jenny G. Sorce. Cosmicflows-3. Astron. J., 152:50, 2016.
- [44] Dan Scolnic et al. The Pantheon+ Analysis: The Full Data Set and Light-curve Release. Astrophys. J., 938(2):113, 2022.
- [45] Adam G. Riess et al. A Comprehensive Measurement of the Local Value of the Hubble Constant with 1 km/s/Mpc Uncertainty from the Hubble Space Telescope and the SH0ES Team. Astrophys. J. Lett., 934(1):L7, 2022.
- [46] Anthony Carr, Tamara M. Davis, Dan Scolnic, Daniel Scolnic, Khaled Said, Dillon Brout, Erik R. Peterson, and Richard Kessler. The Pantheon+ analysis: Improving the redshifts and peculiar velocities of Type Ia supernovae used in cosmological analyses. *Publ. Astron. Soc.* Austral., 39:e046, 2022.
- [47] Erik R. Peterson et al. The Pantheon+ Analysis: Evaluating Peculiar Velocity Corrections in Cosmological Analyses with Nearby Type Ia Supernovae. Astrophys. J., 938(2):112, 2022.
- [48] K. M. Górski, E. Hivon, A. J. Banday, B. D. Wandelt, F. K. Hansen, M. Reinecke, and M. Bartelman. HEALPix - A Framework for high resolution discretization, and fast analysis of data distributed on the sphere. *Astrophys. J.*, 622:759-771, 2005.
- [49] D. J. Fixsen, E. S. Cheng, J. M. Gales, John C. Mather, R. A. Shafer, and E. L. Wright. The Cosmic Microwave Background spectrum from the full COBE FIRAS data set. Astrophys. J., 473:576, 1996.
- [50] R. Brent Tully, Edward J. Shaya, Igor D. Karachentsev, H. M. Courtois, Dale D. Kocevski, Luca Rizzi, and Alan Peel. Our Peculiar Motion Away from the Local Void. Astrophys. J., 676:184–205, 2008.
- [51] Roy Maartens, Chris Clarkson, and Song Chen. The kinematic dipole in galaxy redshift surveys. JCAP, 01:013, 2018.
- [52] Misao Sasaki. The magnitude—redshift relation in a perturbed friedmann universe. Monthly Notices of the Royal Astronomical Society, 228(3):653–669, 1987.
- [53] Camille Bonvin, Ruth Durrer, and M. Alice Gasparini. Fluctuations of the luminosity distance. *Phys. Rev. D*, 73:023523, 2006. [Erratum: Phys.Rev.D 85, 029901 (2012)].
- [54] Ryan J. Turner. Cosmology with Peculiar Velocity Surveys. 11 2024.